

# TEMPERATURE DEPENDENCE OF THE ELECTRONIC BAND GAP OF CsPbBr<sub>3</sub> QUANTUM WELLS OBTAINED USING K•P METHOD

Milan Jocić<sup>1</sup>, Nenad Vukmirović<sup>2</sup>


<sup>1</sup>Department of Physics, Faculty of Sciences and Mathematics,  
University of Niš, Niš, Serbia

<sup>2</sup>Institute of Physics Belgrade, University of Belgrade, Belgrade, Serbia

ORCID iDs: Milan Jocić

Nenad Vukmirović

 <https://orcid.org/0000-0003-4929-9907>

 <https://orcid.org/0000-0002-4101-1713>

**Abstract.** *We calculated the electronic structure of CsPbBr<sub>3</sub> quantum wells using the **k•p** model with parameters extracted from hybrid functional based DFT calculations supplemented with self-energy corrections arising from the electron-phonon interaction. We obtained the temperature dependence of the band gap for different sizes of the quantum well. The results show that the temperature dependence in quantum wells is similar to the one found in bulk phase for all sizes of the well that were considered.*

**Key words:** nanostructure, temperature dependence, quantum well, **k•p** method.

## 1. INTRODUCTION

Since most electronic and optical devices consist of semiconductor materials, there is a great significance in knowing the properties of these materials. Over the years, general improvements of these devices made them smaller in size and more power efficient. Reducing the size from a bulk phase, that can be as small as few micrometers, down to a nanostructure that has a scale of a few dozen nanometers or less introduces a change in electronic properties of the material. This makes it possible to tune the electronic properties, like the band gap of a material, to desired values, allowing us to replicate the electronic properties of a much more expensive or less durable material with a material that is cheaper to produce or more durable. Working with nanostructures whose electronic properties change with their size introduces new challenges for investigating and modeling semiconductor materials.

For the past few decades, density functional theory (DFT) has been routinely used for modeling the properties of the bulk phase of semiconductors with much success, while their nanostructures would prove to be challenging since the required computational

---

Received: January 15<sup>th</sup>, 2024; accepted: December 10<sup>th</sup>, 2024

**Corresponding author:** Milan Jocić

Department of Physics, Faculty of Sciences and Mathematics, Višegradska 33, 18000 Niš, Serbia

E-mail: milan.jocic@pmf.ni.ac.rs

resources are increasing with the size of the nanostructure, and in some cases they become infeasible. Relying on the **k•p** method, alongside DFT, the computational resources required to obtain the electronic structure can be significantly reduced. One disadvantage of the **k•p** is that it considers only several selected bands of interest, while the rest of them are treated perturbatively (like in Löwdin, 1951.). The energy of these bands and their wave-functions have to be extracted from DFT calculation. Another disadvantage is that it can be a good approximation only in a relatively small vicinity around the point in the Brillouin zone from which DFT results are extracted. Since our main interest is the band gap of a nanostructure device, these disadvantages come at an acceptable cost. On the other hand, DFT provides information about all bands in the whole Brillouin zone which is more than sufficient in this case.

Once we determine the size dependent electronic properties of the nanostructure for the desired device, we have to take into account various external conditions that such device would operate under like the surrounding temperature. Both **k•p** and DFT, however, by themselves do not take into account any temperature effects that such devices might be exposed to, and since in practice they are expected to perform at a wide range of outside temperature conditions, these effects should be taken into account as well.

Regarding ab initio modeling of nanostructures, in our previous work (Jocić and Vukmirović 2020.) we provided, among other, a detailed explanation and comparison of DFT and **k•p** methods for bulk and quantum well (QW) nanostructures of CdSe. We have shown that the **k•p** method is in excellent agreement with DFT, even for rather thin QWs, using standard  $8 \times 8$  (H8) and extended  $26 \times 26$  (H26) **k•p** Hamiltonians which take into account the effects of spin-orbit coupling (SOC), which is necessary in the case of heavy ions such as lead.

To determine the effects of temperature on the electronic structure, in our recent paper (Jocić and Vukmirović 2023.) we proposed a method that combines hybrid PBE0 functional based calculation in DFT with the Allen-Heine-Cardona (AHC) theory that provides temperature dependent self-energy correction of electronic bands. Because this self-energy has its origin in electron-phonon interactions it was necessary to obtain proper phonon frequencies, which are also temperature dependent and were obtained using the self-consistent phonon (SCPH) method. Self-energies are then obtained within the AHC theory using the on-the-mass-shell (OTMS) approximation. We also introduced a self-consistent procedure (SCP), which improves upon OTMS approximation, which evaluates these self-energies using interacting Green's functions and extracts the results from the corresponding spectral function. We performed this for several bands below and above the band gap at key points in the first Brillouin zone (1BZ). These methods allowed us to obtain good agreement of the band gap with the available experimental data for  $\text{CsPbCl}_3$ ,  $\text{CsPbBr}_3$  and  $\text{CsPbI}_3$  at zero temperature and the temperature at which transition to cubic phase takes place.

In this work, we turn our attention to perovskite crystal  $\text{CsPbBr}_3$ , and calculate the temperature dependent gap of quantum wells (QW) made from this material. It was observed that  $\text{CsPbBr}_3$  has two phase transitions as temperature increases. At low temperatures it forms an orthorhombic crystal structure that transforms to a tetragonal structure for a narrow range of temperatures, and then transforms to a cubic structure at a temperature of  $T = 403$  K. Since  $\text{CsPbBr}_3$  has recently found application in solar cells, the most interesting region would be the one of high temperatures of the cubic structure at which these solar cells would operate.

In this paper, we combine the method from our previous (Jocić and Vukmirović 2020.) and results from our recent (Jocić and Vukmirović 2023.) work in order to obtain the temperature dependence of band gaps for CsPbBr<sub>3</sub> QW nanostructures. The structure of the paper is as follows: In Theory section, we first provide a brief theoretical overview of the **k**•**p** method for QW nanostructures using a plane wave (PW) basis and discuss the ordering of the bands that go into H8 and H26 Hamiltonians for the cubic structure of CsPbBr<sub>3</sub>. In the Results section, we first demonstrate the procedure for obtaining the convergence of the results with respect to necessary numerical parameters used in **k**•**p** method for QWs. We then present band structure with a more accurate band gap that is obtained from **k**•**p**, using hybrid DFT and temperature corrections for bulk, and a band structure for QW of fixed size using the same parameters. Finally, we show the temperature dependence of the electronic bands and band gaps for QW sizes ranging from around 2 nm to around 18 nm for temperature range from 400 to 700 K.

## 2. THEORY

Constructing a **k**•**p** Hamiltonian for nanostructures requires rewriting equations for bulk in a new form that is suitable for that case. Since the periodicity of the crystal is violated, in the general case, the electron momentum **k** is not a good quantum number anymore and we have to introduce envelope functions  $\psi_m$  alongside Bloch unit cell functions  $u_m$  in the expression for the wave-function  $\Psi$ :

$$\Psi = \sum_m \psi_m u_m. \quad (1)$$

In the case of a cubic CsPbBr<sub>3</sub> lattice, the QW is periodic in the (*x*, *y*) plane, and its size can be determined by counting the number of bulk unit cells along the *z*-direction. We choose the coordinate system in such a way that the QW is located in the region from  $l_1$  to  $l_2$  ( $0 < l_1 < l_2 < L$ ) and the surrounding material is in the region from 0 to  $L$ .

We expand envelopes in PW basis as  $\psi_m(z) = \sum_q W_{mq} a_q$ , where  $a_q(z) = L^{-1/2} \exp(ik_q z)$  are a set of basis functions, and  $k_q = 2\pi q/L$ , with  $q = 0, \pm 1, \pm 2, \pm 3, \dots \pm N_{PW}$ , where  $2N_{PW} + 1$  is the number of plane waves. This makes the envelope function periodic in space as  $\psi_m(z) = \psi_m(z + L)$ . Using the condition that  $\psi_m(r)$  are smooth, continuous, infinitely differentiable and slowly varying functions, whose plane-wave expansion is restricted to the 1BZ and  $u_m(r)$  are a complete set of orthogonal Bloch functions at **k**<sub>0</sub>, periodic over the whole structure, with the periodicity of Bravais lattice (Lew Yan Voon and Willatzen, 2009. ), we arrive at **k**•**p** equations for QWs:

$$\begin{aligned} \sum_{m,q} \left[ \frac{\hbar^2}{2m_0} (\mathbf{k} - \mathbf{k}_0)^2_{(x,y)} \delta_{sq} + \frac{\hbar^2}{2m_0} k_q^2 \delta_{sq} + I^{sq}(E_m) \right] \delta_{nm} W_{mq} \\ + \sum_{m,q} \left[ \frac{\hbar}{m_0} (\mathbf{k} - \mathbf{k}_0)_{(x,y)} \cdot \mathbf{p}_{nm} \delta_{sq} + \frac{\hbar}{m_0} k_q \mathbf{e}_z \cdot \mathbf{p}_{nm} \right] W_{mq} \\ + \sum_{m,q} H_{nm}^{(2)}(s, q) W_{mq} = E W_{ns}, \end{aligned} \quad (2)$$

where  $\mathbf{p}_{nm}$  and  $E_m$  are momentum matrix elements and band energies obtained as **k**•**p** parameters in bulk for **k**<sub>0</sub>,  $m_0$  is the electron mass, and:

$$\begin{aligned}
\Delta k_{sq} &= 2\pi(s - q)/L, \\
I^{sq}(E) &= (E - E_B) I^{sq}(E) \big|_{l_2}^{l_1}, \quad E_B = E \pm \Delta E_B, \\
I^{sq}(E) \big|_{l_2}^{l_1} &= \frac{1}{L} \int_{l_1}^{l_2} e^{-i\Delta k_{sq} z} dz \\
&= \frac{l_1 - l_2}{L} \delta_{sq} + \frac{\delta_{sq} - 1}{iL\Delta k_{sq}} (e^{-i\Delta k_{sq} l_1} - e^{-i\Delta k_{sq} l_2}).
\end{aligned} \tag{3}$$

The second-order perturbation band term  $H_{nm}^{(2)}(s, q)$ , which accounts for remote bands  $r$  that are not present in the first-order Hamiltonian are:

$$\begin{aligned}
H_{nm}^{(2)}(s, q) &= \sum_r \frac{1}{L} \int dz e^{-ik_{sz}} \frac{(\hbar \mathbf{K} \cdot \mathbf{p}_{nr})(\mathbf{p}_{rn} \cdot \hbar \mathbf{K})}{m_0^2[(E_n + E_m)/2 - E_r]} e^{ik_q z} \\
&= \sum_{\alpha, \beta} \frac{1}{L} \int dz e^{-ik_{sz}} \frac{\hbar K_\alpha}{m_0} P_{nm, \alpha\beta} \frac{\hbar K_\beta}{m_0} e^{ik_q z}
\end{aligned} \tag{4}$$

where  $\hbar \mathbf{K} = (\hbar \mathbf{k} - \hbar \mathbf{k}_0)_{(x,y)} + p_z \mathbf{e}_z$ ,  $p_z = -i\hbar \partial_z$  is the momentum operator, and  $P_{nm, \alpha\beta}$  is the second-order  $\mathbf{k} \cdot \mathbf{p}$  momentum tensor. We used  $n, m$  for band indices in bulk and  $\alpha, \beta$  indices for directions  $x, y, z$ .

We assume that the surrounding material has the same parameters as the QW, except for the valence and conduction band energies, that are respectively shifted by  $-\Delta E_B$  and  $+\Delta E_B$  with respect to the QW parameters, where  $\Delta E_B$  is the absolute shift of the bands. This shift is chosen to be large enough to ensure that the wave functions are located in the QW and was set to 10 eV for all our calculations.

Size of the well (surrounding material) is a product of the size of the unit cell in  $z$ -direction  $a$  and some integer  $N$  ( $N_B$ ),  $l = Na$  ( $L = N_B a$ ).  $N_{PW}$  and  $L/l$  are the parameters that need to be studied in more detail, and we will show how to determine them in the next section.

In the limit where  $\mathbf{k}$  is a good quantum number, eqn. (2) transforms to the case of bulk by removing every integration over  $z$ -components and PWs from envelope function expansion, reducing to:

$$\begin{aligned}
&\sum_m \left[ \frac{\hbar^2}{2m_0} (\mathbf{k} - \mathbf{k}_0)^2 + E_m \right] \delta_{nm} W_m \\
&+ \sum_m \left[ \frac{\hbar}{m_0} (\mathbf{k} - \mathbf{k}_0) \cdot \mathbf{p}_{nm} + H_{nm}^{(2)} \right] W_m = E W_m, \\
H_{nm}^{(2)} &= \sum_{\alpha, \beta} \frac{\hbar (\mathbf{k} - \mathbf{k}_0)_\alpha}{m_0} P_{nm, \alpha\beta} \frac{\hbar (\mathbf{k} - \mathbf{k}_0)_\beta}{m_0}.
\end{aligned} \tag{5}$$

Eqn. (2) and eqn. (5) show us how to construct the Hamiltonian, but not which bands and which  $\mathbf{k}$ -point should be used for unperturbed results from DFT. Most of the electronic properties are governed by the symmetry of the crystal and most of the information about the current carriers can be obtained by considering points with the greatest probability for their detection. Extremal states in the electron structure are most likely to have current carriers: holes in the valence band maximum (VBM), and electrons in the conduction band minimum (CBM). Historically, these points and their symmetry have been the center of interest when DFT calculations were not yet computationally feasible, so the electronic

structure was mostly studied by analytical methods in combination with available experimental data. A good overview of these analytical methods can be found in a book by Bir and Pikus, 1974.

The point group of the bulk cubic CsPbBr<sub>3</sub> crystal is  $O_h$ , and the band gap is located at the R-point in the 1BZ. Point group  $O_h$  transforms to a double group, that describes bands when SOC is included, by multiplying all irreducible representations by a spinor representation  $\Gamma_6^+$ . **Fig. 1** illustrates this for bands around the gap in the bulk CsPbBr<sub>3</sub>. When SOC is not included, VBM at R-point is non-degenerate band corresponding to  $\Gamma_2^-$  irreducible representation that transforms to 2-fold degenerate band  $\Gamma_7^-$  when SOC is included. CBM is 3-fold degenerate band at R-point, corresponding to  $\Gamma_5^+$  when SOC is omitted, and transforms by splitting into a 2-fold  $\Gamma_7^+$  with lower energy, now CBM, and 4-fold  $\Gamma_8^+$  band with higher energy, now CBM1. These 8 bands in total make the H8 Hamiltonian.

The larger H26 Hamiltonian is formed when along these 8, we include 3 more valence bands, counting with decreasing energies from VBM: 4-fold  $\Gamma_8^-$ , 2-fold  $\Gamma_7^-$ , and 4-fold  $\Gamma_6^-$ , respectively, and 3 more conduction bands, counting with increasing energies from CBM1: 2-fold  $\Gamma_6^+$ , 2-fold  $\Gamma_7^+$ , and 4-fold  $\Gamma_8^+$ , respectively.

Both H8 and H26 have a unique set of **k**·**p** parameters that consist of energies  $E_m$ , momentum matrix elements  $\mathbf{p}_{nm}$  and second-order momentum tensors  $P_{nm,\alpha\beta}$ . Using the same parameters for bulk, we construct the H26 Hamiltonian for QW from eqn. (2), taking note that the periodicity is now valid only in the (*x*, *y*) plane.

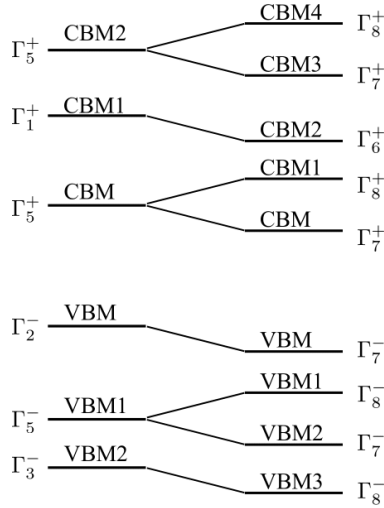


**Fig. 1** Ordering of the bands around the gap and their transformation when SOC is included. Distance between the bands does not scale with energy distance between them. Notation for the irreducible representations that was used here follows the one found in Bradley and Cracknell, 2010.

## 3. RESULTS AND DISCUSSIONS

Depending on the size of the  $\mathbf{k} \cdot \mathbf{p}$  Hamiltonian, a small change of numerical parameters  $L/l$  and  $N_{PW}$  can have a significant effect on the result. This is especially true for smaller wells, while large wells that approach bulk in terms of size are less sensitive to those changes. For this reason, we inspect the convergence with respect to those parameters as follows. First, we fix some  $l$ , and gradually increase the size of the surrounding material  $L$  and number of plane waves  $N_{PW}$  until we achieve convergence. This process is repeated for every  $l$ .

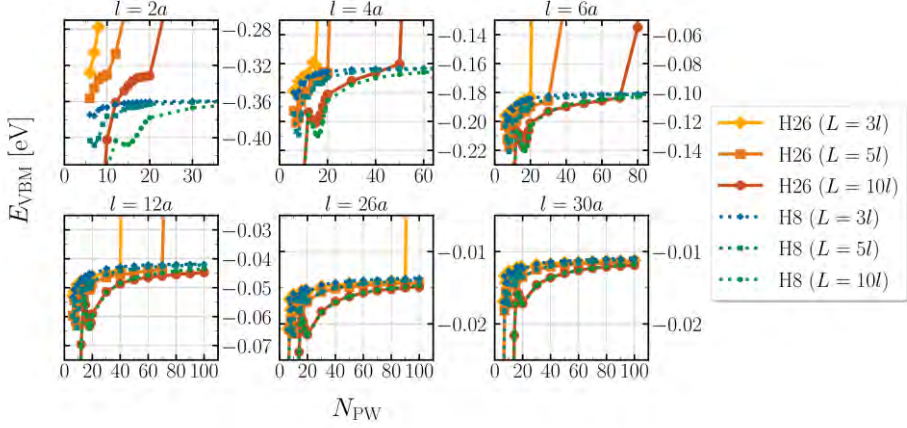


**Fig. 2** Energy of VBM as a function of  $N_{PW}$ , in QWs. The results were obtained using H26 (solid lines) and H8 (dotted lines) Hamiltonians, respectively, for QWs of the size  $l=2a$ ,  $l=4a$ ,  $l=6a$ ,  $l=12a$ ,  $l=26a$ ,  $l=30a$  in units of the lattice constant  $a$ . The size of the surrounding material is  $L=3l$  (diamonds),  $L=5l$  (squares), and  $L=10l$  (circles).

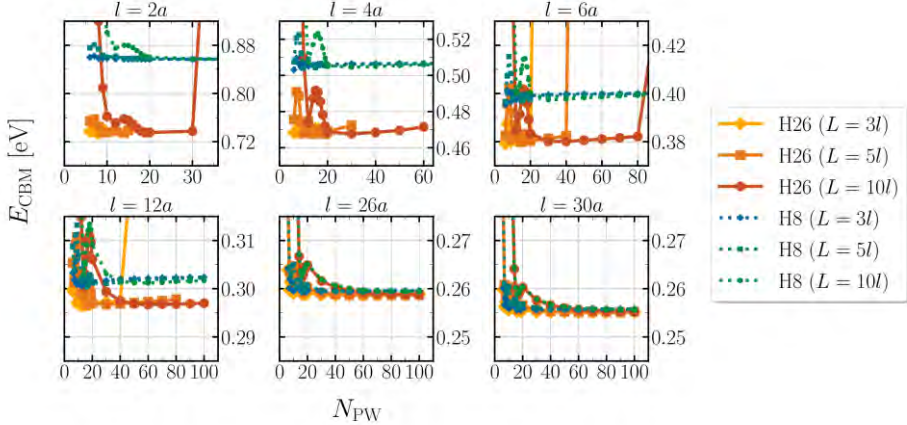


**Fig. 3** Energy of CBM as a function of  $N_{PW}$ , in QWs. The results were obtained using H26 (solid lines) and H8 (dotted lines) Hamiltonians, respectively, for QWs of the size  $l=2a$ ,  $l=4a$ ,  $l=6a$ ,  $l=12a$ ,  $l=26a$ ,  $l=30a$  in units of the lattice constant  $a$ . The size of the surrounding material is  $L=3l$  (diamonds),  $L=5l$  (squares), and  $L=10l$  (circles).

We will focus on H8 and H26 **k**•**p** Hamiltonians, both of which we first construct for bulk from DFT results using PBEsol functional as described in Jocić and Vukmirović 2020. and eqn.(2). For DFT calculation we used a  $4 \times 4 \times 4$  **k**-grid for electron states, electron kinetic energy cutoff of 50 Ry, and a total of 240 bands for cubic phase of CsPbBr<sub>3</sub> with a lattice constant of  $a = 11.1 a_0$  (where  $a_0$  is the first Bohr radius). DFT calculations were performed with included SOC. Since we are most interested in the position of VBM and CBM, and therefore the band gap, we will focus our convergence tests on these bands.

In Fig. 2 (Fig. 3) we present the energy of the VBM (CBM), as a function of  $N_{PW}$ , respectively. The resulting band gap is presented in Fig. 4. All three figures show results for small ( $l = 2a$  and  $l = 4a$ ), intermediate ( $l = 6a$  and  $l = 12a$ ) and large ( $l = 26a$  and  $l = 30a$ ) QWs, respectively.

Although the **k**•**p** method for QWs itself does not require much computational resources and it can be done, on a single-core desktop computer, it is important to estimate, for every  $l$ , at which point increasing  $L/l$  and  $N_{PW}$  does not change the results of the band gap by more than 10 meV. For H8 one usually needs a smaller ratio of  $L/l$ , and for  $L/l = 3$ , the  $N_{PW}$  of 10, 20, 30, 40 and 40, for  $l = 2a, l = 4a, l = 12a, l = 26a$ , and  $l = 30a$ , respectively, was sufficient. For H26 one usually needs a larger  $L/l$  ratio for smaller wells, while larger wells that approach bulk can have acceptable results for a smaller size of the surrounding material. For  $l = 2a$  and  $l = 4a$ , it was sufficient to use  $N_{PW} = 16$  and  $N_{PW} = 30$ , respectively with  $L/l = 10$ . For  $l = 6a$  and  $l = 12a$ , it was sufficient to use  $N_{PW} = 20$  and  $N_{PW} = 40$ , respectively with  $L/l = 5$ . For  $l = 26a$  and  $l = 30a$ , it was sufficient to use  $N_{PW} = 30$  and  $L/l = 3$ .

For small QWs, the results for band gaps obtained from H8 and H26 can differ as much as 150 meV (see Fig. 4), with H8 overestimating the band gap with respect to H26. For intermediate and large QWs, difference in band gaps between H8 and H26 is still present, although it is much smaller and does not exceed 15 meV and 2 meV, respectively.

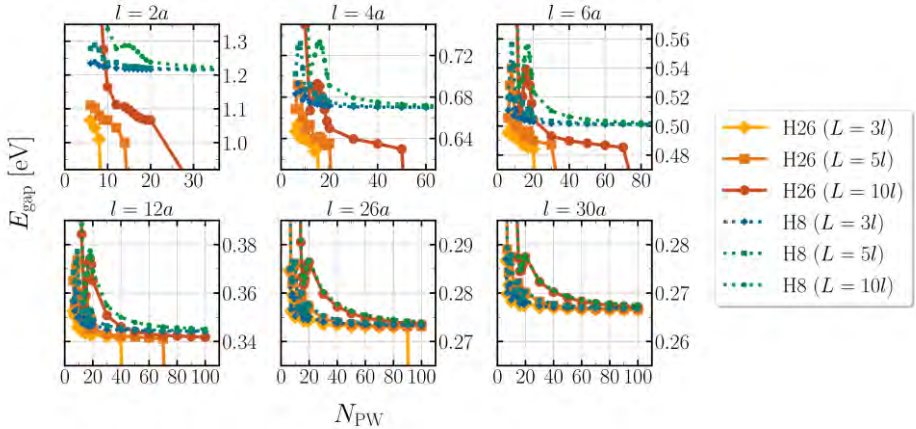


**Fig. 4** Energy of the band gap as a function of  $N_{PW}$ , in QWs. The results were obtained using H26 (solid lines) and H8 (dotted lines) Hamiltonians, respectively, for QWs of the size  $l = 2a, l = 4a, l = 6a, l = 12a, l = 26a, l = 30a$  in units of the lattice constant  $a$ . The size of the surrounding material is  $L = 3l$  (diamonds),  $L = 5l$  (squares), and  $L = 10l$  (circles).



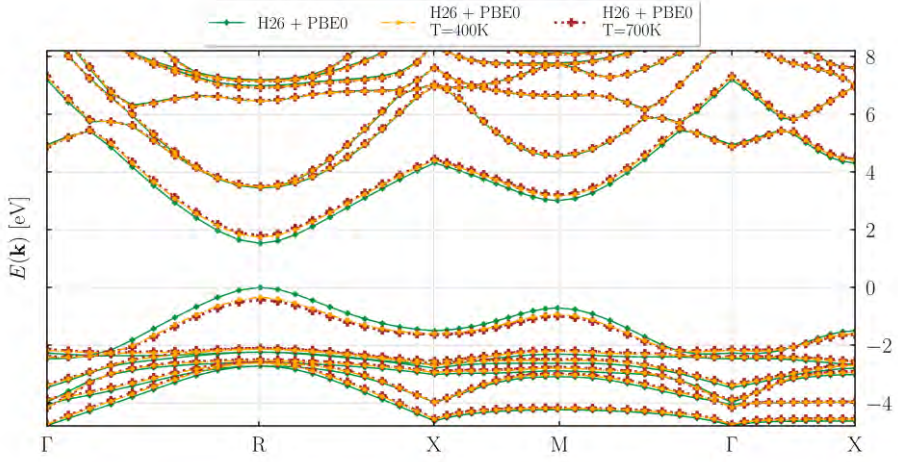


**Fig. 5** The band structure of bulk  $\text{CsPbBr}_3$  obtained using H26 Hamiltonians, replacing  $E_m$  with  $E_m^{PBE0}$  (solid line with diamonds) and with  $E_m^{PBE0} + \Sigma_m(T)$  correction from SCP calculations at  $T = 400$  K (dash-dot line with circles) and  $T = 700$  K (dotted line with crosses), respectively.

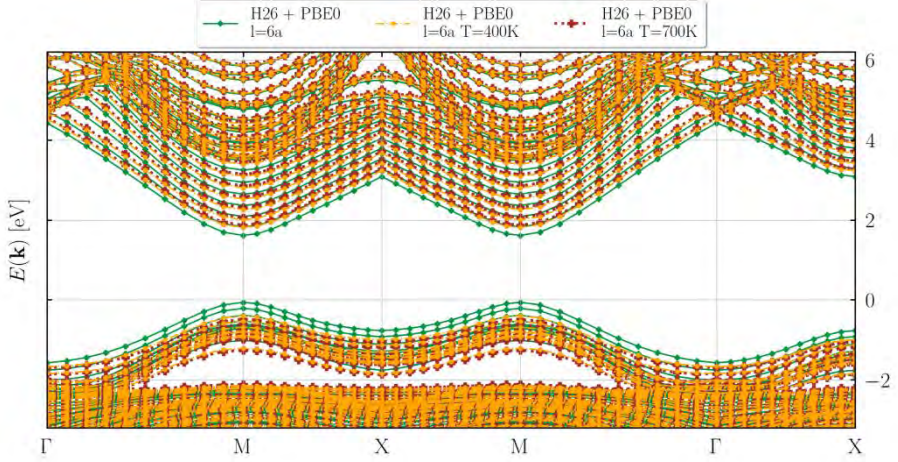


**Fig. 6** The band structure of  $\text{CsPbBr}_3$  QW of size  $l = 6a$  obtained using H26 Hamiltonians replacing  $E_m$  with  $E_m^{PBE0}$  (solid line with diamonds) and with  $E_m^{PBE0} + \Sigma_m(T)$  correction from SCP calculations at  $T = 400$  K (dash-dotted line with circles) and  $T = 700$  K (dotted line with crosses), respectively.

In eqn. (2), we restrict envelope functions to the expansion on plane-waves only in the 1BZ. Therefore, in the general case, one would expect some kind of divergence for both H8 and H26, when  $N_{PW} > L/a$  or equivalently when  $N_{PW} > N_B$ . However, due to having much less parameters than H26, H8 seems to be stable even when  $N_{PW} > N_B$  unlike H26



which shows divergence in this case, as seen in Fig. 2, Fig. 3 and Fig. 4. We also note that H8 always converges before  $N_{PW}$  exceeds the limits of the 1BZ. However, for large wells, both H8 and H26 require less plane-waves than are needed to fill the whole 1BZ, in order to calculate the band gap. For these reasons, we can also check the convergence, by fixing the  $N_{PW} = N_B$  to always include all plane-waves in the 1BZ, while only increasing the size ratio of the surrounding material and the QW  $L/l$ , and then checking if the resulting band gap changes with reduction of  $N_{PW}$ .

Since DFT has a well-documented problem that it typically underestimates the band gaps (Perdew, 1985.), we can improve our **k**·**p** results by replacing DFT bulk PBEsol energies with the ones obtained using PBE0 (Perdew, 1996.) to obtain a more accurate gap. To include the temperature correction, we add the electron self-energy correction  $\Sigma_m(T)$  that comes from the electron-phonon interaction. When calculating PBE0 energies  $E_m^{PBE0}$ , we used the same numerical parameters as previously mentioned for PBEsol, with the addition of  $4 \times 4 \times 4$   $q$ -grid for sampling the required Fock operator and we used the Gygi-Baldereschi method to treat the singularity at  $q \rightarrow 0$ . Results for  $\Sigma_m(T)$  were used from our recent paper (Jocić and Vukmirović 2023.), where we used the maxima of the spectral function from SCP method to obtain band energy corrections. The results are available for temperatures from  $T = 400$  K to  $T = 700$  K.

In eqn. (5), we replace all  $E_m$  with  $E_m^{PBE0}$ , for H26 without temperature correction, and with  $E_m^{PBE0} + \Sigma_m(T)$  for  $T = 400$  K and  $T = 700$  K, respectively, to include temperature effects in bulk. The resulting band dispersion plot is presented in Fig. 5. As expected from our recent work the biggest shift in energies is observed for VBM and CBM (when comparing against other bands that form H26), which effectively gives the band gap of 2.08 eV and 2.23 eV at  $T = 400$  K and  $T = 700$  K, respectively, and 1.5 eV without the  $\Sigma_m(T)$ . Inserting the same parameters in eqn. (2), we obtained the band gaps of 1.67 eV, 2.21 eV and 2.35 eV, respectively for QW of size  $l = 6a$  with its band dispersion shown in Fig. 6.

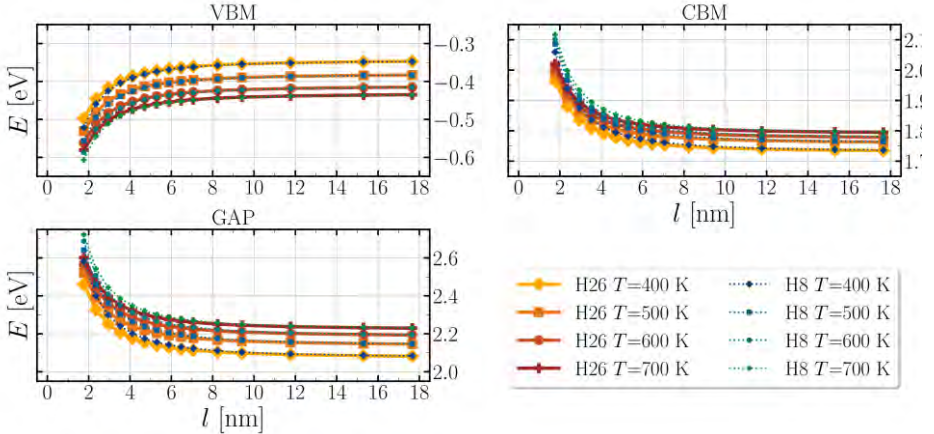


**Fig. 7** Energies of VBM, CBM and band gaps for CsPbBr<sub>3</sub> QW as a function of the size of the QW  $l$ , obtained using H26 Hamiltonian (solid lines) and H8 (dotted lines) when  $E_m$  is replaced by  $E_m^{PBE0} + \Sigma_m(T)$ , at temperatures of  $T = 400$  K (diamonds),  $T = 500$  K (squares),  $T = 600$  K (circles),  $T = 700$  K (crosses).

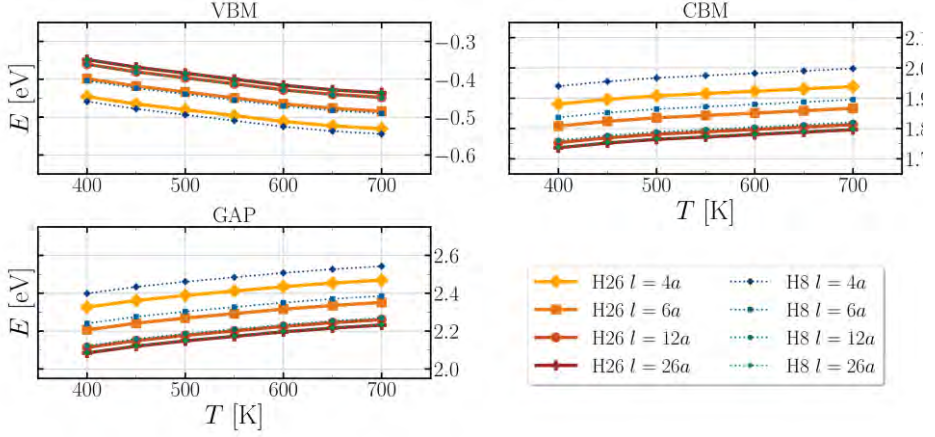


**Fig. 8** Energies of VBM, CBM and band gaps for CsPbBr<sub>3</sub> QW as a function of temperature  $T$ , obtained using H26 Hamiltonian (solid lines) and H8 (dotted lines) when  $E_m$  is replaced by  $E_m^{PBE0} + \Sigma_m(T)$ , respectively for several sizes of QWs  $l = 4a$  (diamonds),  $l = 6a$  (squares),  $l = 12a$  (circles),  $l = 26a$  (crosses) in units of lattice constant  $a$ .

Finally, we present the temperature dependence of QW band gaps using H26 and H8 Hamiltonians. We calculated how energies of VBM, CBM, and the band gap change with the size of the QW and temperature, respectively. The  $E = 0$  level is the one VBM takes for the bulk phase with  $E_m^{PBE0}$  energy set. Consistent with the previous figures, H26 and H8 give almost identical results for intermediate and large QWs, while they show a slight discrepancy for small QWs.

Fig. 7 shows energies of VBM, CBM, and band gaps, respectively, as a function of QW size  $l$ , starting from  $l = 2a$  and going to  $l = 30a$  for several temperatures that range from 400 to 700 K. From this figure we can conclude that the energies of the bands and therefore the gap change significantly with the increase of the QW size until certain point (around 8 nm), after which the results very slowly approach the same ones found in the bulk phase.

Fig. 8 shows energies of VBM, CBM, and band gaps, respectively, for temperatures from  $T = 400$  K to  $T = 700$  K for several QW sizes of  $l = 4a$ ,  $l = 6a$ ,  $l = 12a$ , and  $l = 26a$ . From this figure we can see that the relative change of energies with temperature is similar for all sizes of QWs and again similar for bulk when compared to results from Jocić and Vukmirović 2023.

#### 4. CONCLUSION

In this work, we demonstrated a procedure for obtaining convergence with respect to numerical parameters used for H8 and H26 **k**•**p** Hamiltonians for QWs like the size ratio of the surrounding material and the QW of width  $L/l$  and the number of plane waves in the envelope function expansion  $N_{PW}$ , relying on the procedure used in Jocić and Vukmirović 2020. We demonstrated that even when H8 shows no divergence for  $N_{PW} > N_B$ , the results do not change from the ones that take all plane-waves in the 1BZ. The H26 produces

diverging results whenever  $N_{PW} > N_B$ , but for large QWs a good result can be obtained when  $N_{PW} < N_B$ . We obtained a band dispersion with improved value for the band gap for bulk and QW, using H26 and replacing PBEsol energies  $E_m$  with PBE0 energies  $E_m^{PBE0}$  and then introducing the temperature effects from electron self-energy corrections  $\Sigma_m(T)$ , obtained from spectral function maxima, as in Jocić and Vukmirović 2023. Finally, we obtained results for the temperature dependence of band gaps for QWs using the **k**•**p** method. Band gap results were obtained for wells in the range from  $l = 2a$  to  $l = 30a$ , and for the temperatures from 400 K to 700 K. This way, we showed how the band gap of the QWs changes with size and temperature in the case of perovskite CsPbBr<sub>3</sub> in cubic form.

**Acknowledgments.** We acknowledge funding provided by the Institute of Physics Belgrade, through the grant by the Ministry of Science, Technological Development and Innovation of the Republic of Serbia. Numerical computations were performed on the PARADOX-IV supercomputing facility at the Scientific Computing Laboratory, National Center of Excellence for the Study of Complex Systems, Institute of Physics Belgrade.

## REFERENCES

- Bir, G., Pikus, G., *Symmetry and Strain-induced Effects in Semiconductors*, Wiley, New York, 1974.  
 Bradley, C., Cracknell, A., *The Mathematical Theory of Symmetry in Solids: Representation Theory for Point Groups and Space Groups*, Oxford University Press, Oxford **2010**.  
 Jocić, M., Vukmirović, N., 2020. Phys. Rev. B, 102, 085121. doi: 10.1103/PhysRevB.102.085121  
 Jocić, M., Vukmirović, N., 2023. Phys. Chem. Chem. Phys., 25, 29017–29031, doi: 10.1039/D3CP02054A  
 Lew Yan Voon, L. C., Willatzen, M., *The **k**•**p** Method: Electronic Properties of Semiconductors*, Springer-Verlag, Berlin Heidelberg, **2009**.  
 Löwdin, P., 1951. J. Chem. Phys., 19, 1396–1401, doi: 10.1063/1.1748067  
 Perdew, J. P., 1985. Int. J. Quantum Chem., 28, 497–523, doi: 10.1002/qua.560280846  
 Perdew, J. P., Burke, K., Ernzerhof, M., 1996. Phys. Rev. Lett., 77, 3865–3868, doi: 10.1103/PhysRevLett.77.3865

## TEMPERATURSKA ZAVISNOST ELEKTRONSKOG ENERGETSKOG PROCEPA KVANTNIH JAMA CsPbBr<sub>3</sub> DOBIJENIH POMOĆU **k**•**p** METODA

*Izračunali smo elektronsku strukturu CsPbBr<sub>3</sub> kvantne jame pomoću **k**•**p** modela korišćenjem parametara iz DFT proračuna na bazi hibridnih funkcionala sa dodatkom korekcija za self-energije koje potiču od elektron-fonon interakcije. Dobili smo temperatursku zavisnost procepa za različite veličine kvantne jame. Rezultati pokazuju da je temperaturska zavisnost u kvantnim jamama, za sve veličine jama koje su uzete u obzir, slična onoj koja se dobija za balk fazu.*

**Ključne reči:** nanostrukture, temperaturska zavisnost, kvantne jame, **k**•**p** metoda.